Atmospheric Research 194 (2017) 100–108

Contents lists available at ScienceDirect

Atmospheric Research

journal homepage: www.elsevier.com/locate/atmosres

Effect of relative humidity on the deposition and coagulation of aerosolized SiO_2 nanoparticles

Youfeng Wang, Lan Chen*, Rui Chen, Guolan Tian, Dexing Li, Chunying Chen, Xiujie Ge, Guanglu Ge*

CAS Key Laboratory of Standardization and Measurement for Nanotechnology, CAS Center for Excellence in Nanoscience, National Center for Nanoscience and Technology, Beijing, 100190, PR China

ARTICLE INFO

Keywords:
Aerosol
SiO_2 nanoparticles
Particle deposition
Coagulation
Relative humidity (RH)

ABSTRACT

The temporal evolution of aerosolized SiO_2 nanoparticles (NPs) released into an environmental test chamber has been investigated to interrogate the effect of relative humidity (RH) on the deposition and coagulation of the nanoparticles. The size-resolved deposition rate and Brownian coagulation coefficient for the particles at RH of ~10%, 27%, 40%, 54%, and 64% are estimated. The results show that the effect of RH on the deposition rate is size-dependent; for particle diameter (Dp) < 70 nm, the deposition rate reduces as the RH rises; while for Dp > 70 nm, it grows as the RH rises. Generally, both low and high RH tends to enhance the deposition rate, and the minimum rate appears at moderate RH (~54%). Electrostatic repulsion is probable for the inter-particles interaction at the low RH while the surface roughness due to water molecular adsorption is a main reason for the particle-wall interaction at higher RH. The increasing coagulation coefficient at high humidity correlates to the strong inter-particle adhesion, which may be caused by the water molecular adsorption on the hydrophilic surfaces of the SiO_2 NPs due to the formation of nanometer-thick water film. This study suggests that air humidity plays unignorable roles in particle deposition and coagulation.

1. Introduction

The indoor aerosol formed by engineered nanoparticles (ENPs) causes great concerns about occupational health and environmental safety and recently have attracted more and more attentions due to their broad scope of existence and applications. (Martin et al., 2015; Sotiriou et al., 2015; Friedlander and Pui, 2004). A number of toxicological studies have indicated that nanoparticles may cause some pulmonary and cardiovascular diseases due to their huge specific surface area, which is easier to carry more toxic air pollutants compared with the particles at microscale (Bräuner et al., 2007; Stölzel et al., 2007).The risk for human exposure to the indoor airborne nanoparticles is correlated to the size and number concentration of the particles, and governed by the strength of its emission sources, air filtration efficiency, air ventilation and particle dynamics etc. It is, therefore, highly desired to have better understanding on the environmental behavior of the nanoparticles and other factors.

Particle deposition and coagulation (D/C) are widely accepted as two major mechanisms to describe the overall particle dynamics in an enclosed aerosol system. Many groups have studied D/C as the function of particle size distribution and concentration (Jamriska and Morawska, 2003; Maynard and Zimmer, 2003; Schnell et al., 2006).The key information and parameters obtained from the particle D/C studies are important and useful since the establishment of many indoor air quality (IAQ) models (Allard et al., 1990; Guo, 2000) requires this kind of information, e.g. deposition rate and coagulation coefficient. Previous studies have shown that the factors to affect the particle deposition on the surfaces of an enclosed chamber are particle characteristics (e.g. particle size, size distribution), airflow patterns, the geometry and surface feature of the enclosed chamber (Zhao and Wu, 2007; Lai, 2002; Liu, 2009). Brownian and turbulent diffusion are considered as the major factors to influence the deposition process of ultrafine particles (< 0.1 μm), and gravitational settling is more significant for the particles larger than 1 μm, while the dominant mechanism for those between 0.1–1 μm is not quite clear, where typical V-shaped curve of the deposition rate vs size is observed (Nazaroff, 2004; Lai and Nazaroff, 2000). Particle coagulation more easily happens for the ultrafine particles with higher concentration due to higher probability for the particle-particle collisions compared with the larger ones, where the particle size, Brownian motion, Van der Waals force, viscosity, and aggregate state are the main factors to be considered to affect the coagulation (Rim et al., 2012; Yu et al.,

* Corresponding authors.
E-mail addresses: chenlan@nanoctr.cn (L. Chen), gegl@nanoctr.cn (G. Ge).

http://dx.doi.org/10.1016/j.atmosres.2017.04.030
Received 13 October 2016; Received in revised form 11 January 2017; Accepted 19 April 2017
Available online 21 April 2017

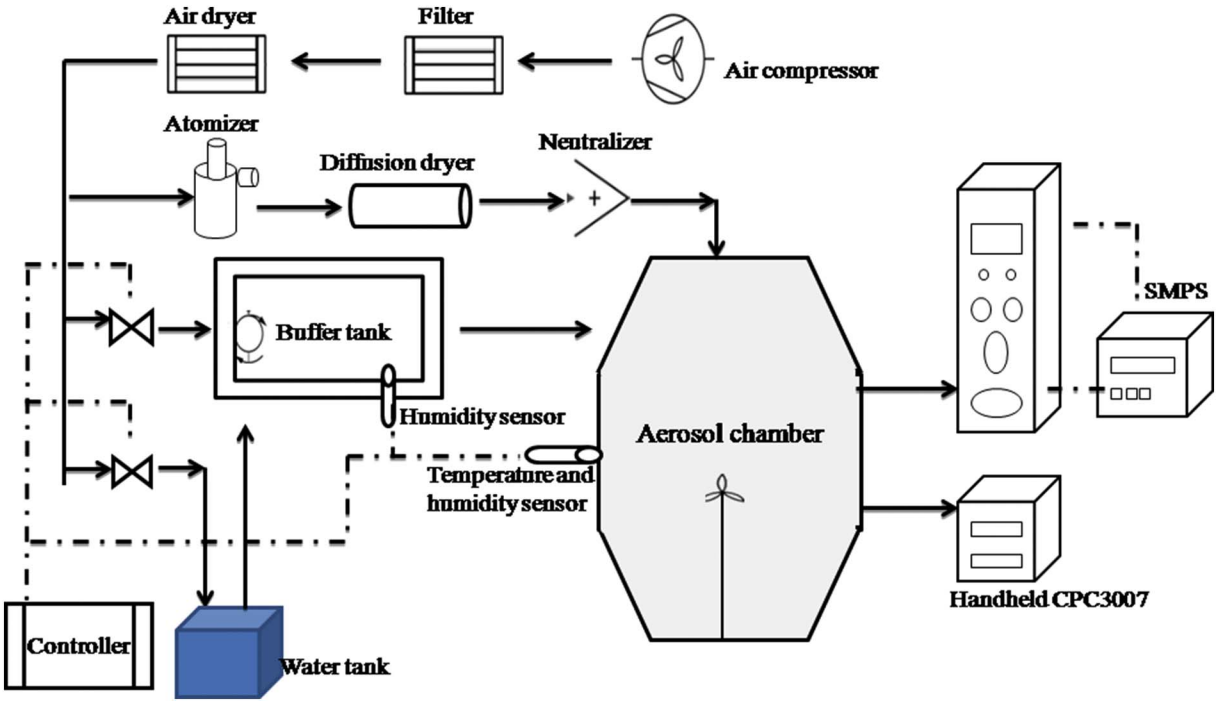

Fig. 1. Scheme for the experimental setup.

2013). The coagulation of polydisperse nanoparticles has been investigated in several pioneering studies through experimental measurements and numerical simulations (Kim et al., 2003; Lee and Chen, 1984; Buesser et al., 2009; Otto et al., 1999). The D/C mechanisms and their correlation have been intensively investigated before (Yu et al., 2013; Jamriska and Morawska, 2003).

Most D/C mechanism researches focus on the experimental conditions such as ventilation system, air exchange rate, temperature, and/or stirring speed (Zhao et al., 2015; Hussein et al., 2009a; Schnell et al., 2006; Maynard and Zimmer, 2003; Lee et al., 2014). Few studies take the impact of relative humidity (RH) on particle D/C under consideration. The effect of RH on the D/C rate is elusive, due to the complex interplay between surface condensation, adhesion and air viscosity. Morawska et al. (1997) have observed the behavior of the environmental tobacco smoke at varying RHs from 42% to 95% and found the increase in particle size at higher RH, but further analysis on the D/C rate is neglected. Ostraat et al. (2010) have investigated several experimental variables including chamber RH on the aging of polydisperse SiO_2 NPs. Because of small chamber volume (1.5 L and 15 L) and short residence time, no remarkable difference for the size distribution and efficiency loss has been observed for the SiO_2 NPs at RH of 0% and 30%, respectively. Atmospheric RH condition is well-known to affect the transformation process of the NPs e.g. the gas-to-particle conversions, aging and physico-chemical properties of the particles (Jamriska et al., 2008; Wehner et al., 2002). Aerosol hygroscopicity referring to the uptake of water molecules by particles in response to increasing RH is essential for the formation of cloud condensation nuclei, and thus has drawn greater attentions in assessing their impact on weather-climate effect and atmospheric visibility (Jiang et al., 2016; Liu et al., 2011). Abundant experimental evidences have shown that the RH plays a key role on changing the morphology and dispersion state of fine particles due to aggregation and eventually influencing the performance of the particle filters (Montgomery et al., 2015a,b; Miguel, 2003). Therefore, more comprehensive researches are required to investigate and assess the RH effect on the D/C rates.

Hence, this study aims to experimentally investigate the temporal decay behavior for polydisperse aerosol under various RH conditions. Two set of instruments work simultaneously to control the initial concentration and measure the particle concentration decay during the same time, where the aerosol is well-mixed and kept statically prior to the measurement in a chamber. A semi-empirical model and a regression method have been employed to derive the D/C rate and then compared with those reported in literature. The effect of RH on D/C rate provides a reference to further analyze the environmental behavior of the airborne NPs and evaluate the potential risk of human exposure to ENPs.

2. Experiment

2.1. Experimental set-up

The experimental chamber of volume $\sim 0.42\ m^3$ ($S \sim 3.3\ m^2$) is composed of stainless steel and poly (methyl methacrylate) (PMMA). One inlet and two outlets used for injecting and sampling are mounted on the upper and lower wall of the chamber respectively. To on-line monitor the temperature and the RH in the chamber, a temperature and a humidity sensor with an accuracy of ± 0.5 °C for the temperature and ± 2.5% for the humidity are installed through a narrow hole on the vertical surface of the chamber and connected to the humidity control module. The humidity control module consists of a proportional-integral-differential (PID) controller, a water tank, a buffer tank and a humidity sensor. It is used to record and adjust the chamber humidity to the targeting humidity by regulating and controlling the flow rate of the moistened and dried air via the PID controller. The temperature of the chamber is monitored but not controlled during the experiments. Logging intervals were set at 1 s for the temperature and the RH throughout the experiments. A steel fan with a diameter of 10 cm is equipped in the middle for gentle mixing before the sampling begins. No extra treatment is applied for the slightly rough inner surface and the shell of the chamber to minimize the deposition of aerosol particles. The scheme of the experimental set-up is shown in Fig. 1.

2.2. Aerosol generation

Polydisperse silica (SiO_2, $2.2\ g\ cm^{-3}$) aerosol are generated via a six-jet collision atomizer (TSI model 9306) under an inlet pressure of

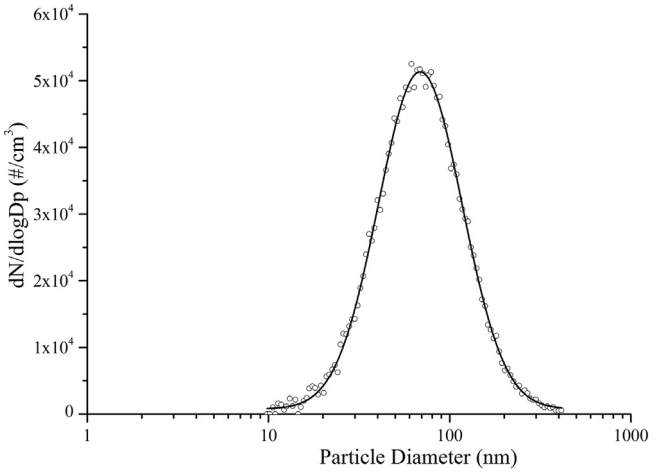

Fig. 2. Particle size distributions (PSDs) of the aerosolized SiO_2 nanoparticles in the chamber measured by SMPS.

25 psi, followed by passage through a diffusion dryer (a drying system filled with 3A molecular sieves) and an electrical charge neutralizer (TSI model 3087) before being introduced into the test chamber and mixed with the air with a targeting RH. The SiO_2 nanoparticles were synthesized in acetone by a patented technology developed by us (Chen et al., 2016) using tetraethyl orthosilicate (TEOS) as the precursor, and tetramethylammonium hydroxide (TMAH) as the catalyst. The SiO_2 colloidal suspensions were prepared by dispersing a given amount of SiO_2 powder into ultrapure water by ultrasonic probe. These processes enable the production of stable polydisperse SiO_2 aerosol particles with ideal Log-normal size distribution, ranging from 10 to 400 nm, as shown in Fig. 2.

SiO_2 particles are one of the main workplace exposures in industrial environment due to their easy production and wide applications, where SiO_2 is stable and almost non-hygroscopic in nature. The mechanisms involved in the dynamics of the aerosolized nanoparticles are mainly surface deposition and coagulation, other processes such as hygroscopic growth, deliquesce, evaporation/condensation is not considered under the experimental conditions. Due to the ease to modify their surface properties, such as making hydrophilic surfaces by terminating with –OH groups and hydrophobic ones by terminating with $–H/CH_3$ groups, the SiO_2 NPs is an ideal model to study the deposition-only and coagulation-only behaviors for the particles with the same size under comparable conditions. For the hygroscopic particles, the results may be quite different due to structural collapse or conglomeration of the aerosol particles on exposure to elevated RH (Montgomery et al., 2015b).

2.3. Measurement scenario

Five targeting RHs in the range of 5%–66% (RH = 10%, 27%, 40%, 55%, and 65%) are maintained in the chamber to determine the relationship of the D/C with different sized ultrafine particles. Before each measurement, the chamber is rinsed with ultrapure water, wiped with dust-free paper, and flushed with filtered air at a targeting RH at a feed rate of 20 L/min via the humidity control module in order to obtain a particle-free environment (background particle concentration $< 300\ cm^{-3}$). Aerosol particles are then injected into the chamber through the inlet at a well-controlled flow rate as long as the RH in the chamber is maintained at the targeting value. When the aerosol particles reached to the desired number concentration, the aerosol generator is stopped and the consecutive particle sampling starts. In prior to the sampling, the aerosol is kept gentle stirring to make the particles well-mixed. The chamber is connected to the buffer tank at the same RH to maintain a constant pressure inside the chamber.

In a closed system, coagulation is always accompanied by deposition, and the deposition-only experiments are conducted prior to the coagulation experiments under the similar experimental conditions. It has been reported that high particle number concentration would result in coagulation. Rim et al. (2012) suggested that the coagulation effect should be accounted for the ultrafine particles at the concentration high than $2.0 \times 10^4\ cm^{-3}$. Therefore, particle concentrations below $2.0 \times 10^4\ cm^{-3}$ are used in this study to investigate the size-resolved deposition-only behavior at different RHs, where the coagulation is considered to be negligible. In addition, higher particle concentrations of $\sim 6.0 \times 10^4\ cm^{-3}$ are also applied to ensure the co-existence for both the coagulation and deposition, where both of them have significant effect on the total particle decay. To minimize the uncertainty of the particle concentration fluctuation, each decay measurement is repeated for three times at each targeting RH under both low- and high-concentration conditions. Detailed information concerning the low- and high-concentration experiments is shown in Tables S1 and S2 in the Supporting information.

The particle size distributions (PSDs) are measured by a Scanning Mobility Particle Sizer (SMPS, TSI model 3936, USA; sample flow rate: 0.6 L/min, sample to sheath flow ratio: 1:10), mounted with a water-based Condensation Particle Counter (CPC, TSI model 3788, USA), an Electrostatic Classifier (EC, TSI model 3080, USA), and a Differential Mobility Analyzer (DMA, TSI model 3081, USA). The total particle number concentration (TNC) is monitored on-line by a hand-held Condensation Particle Counter (CPC, TSI model 3007, USA; sample flow rate: 0.7 L/min). The results of the real-time monitored TNC are shown in Figs. S1 and S2 (Supporting information). The size detection range for SMPS and hand-held CPC in this study is 10 to 414 nm and 10 to 1000 nm plus, respectively and the upper concentration range is 1.0×10^7 and 1.0×10^5 particles cm^{-3}, respectively. The particle number concentration in this work is controlled below 1.0×10^5 particles cm^{-3} without coincidence correction. Zero calibration with high efficiency particulate air filter (HEPA) is conducted for the two instruments before use. Both the SMPS and the CPC3007 sample through an external silicone conductive tubing (1 m long and 1/4 in. inner diameter) and the counting interval is 3 min. The data presented here is corrected by the penetration efficiency for the particles according to the particle loss caused by sampling (Hinds, 1999). For each targeting RH, the particle decay test continues for about 2 h to determine the size-resolved deposition rate and continues for another 1 h to analyze the Brownian coagulation in the case of high-concentration experiment. The total sampling volume during the experiments is ~25% and ~13% of the chamber volume for both the low- and high-concentration experiments, respectively. Previous studies by Rim et al. (2012) and Schnell et al. (2006) have demonstrated that the particles removed by the sampling, which are accounted as ventilation losses, do not significantly affect the coagulation and deposition process under still conditions (< 5%). Therefore, the deviation caused by the sampling outflow on the particle decay behavior is not considered in this study.

3. Results and discussion

3.1. Data analysis

Our analyses use semi-empirical estimation of the size-resolved deposition rate, the mass balance approach to derive the separated contribution of D/C, and the least-error-square algorithm regression to obtain the time-averaged deposition rate and coagulation coefficient, as the function of RH.

Particle data are divided into 10 size categories, < 30, 30–40, 40–50, 50–60, 60–70, 70–85, 85–100, 100–150, 150–200, and > 200 nm. In addition, the total particle concentration in low-concentration experiment is used to analyze size-resolved deposition rate k_i at various RH conditions. We estimated k_i based on Eq. (1) assuming the re-

suspension, condensation/evaporation and coagulation processes ignorable under the experimental conditions:

$$\frac{dC(v_i,t)}{dt} = -k_i C(v_i,t) \quad k_i = -\frac{\ln\frac{C(v_i,t)}{C(v_i,0)}}{t} \tag{1}$$

where $C(v_i, t)$ is the particle concentration of a certain particle size fraction in the i^{th} size category at time t, (particles cm^{-3}) and k_i is the deposition rate for the particles in the i^{th} size category (s^{-1} or h^{-1}). Then Eq. (1) is used and the temporal variation of aerosol concentration is regressed against time by the least square method. The obtained slope from the best-fit line denotes the estimated deposition rate k_i.

In the case of the coagulation and deposition occurred simultaneously in a closed chamber with high-concentration, the general form of the mass balance can be expressed by the following equation (Zhao et al., 2015):

$$\frac{dC(v_i,t)}{dt} = -k_i C(v_i,t) + \frac{1}{2}\sum_{j=1}^{i}\beta_{v_i-v_j,v_j}C(v_i-v_j,t)C(v_j,t) - C(v_i,t)\sum_{h=1}^{n}\beta_{v_i,v_h}C(v_h,t) \tag{2}$$

The term on the left-hand-side of Eq. (2) represents the size-resolved particle number concentration decay; the first term on the right-hand-side represents the particle loss of the i^{th} size category due to surface deposition, the second term gives the production rate of particle size v_i by the collision of particle size $v_i - v_j$ and v_j, and the third term represents the reduction rate of particle size v_i by the collision with the particles of all sizes. Due to the complexity of the pair to pair nanoparticle collision and coagulation theory, we adopt a simplified equation according to Kim et al. (2003):

$$\frac{dC(t)}{dt} = -k\,C(t) - \gamma\,C(t)^2 \tag{3}$$

Combining Eqs. (1), (2) and (3),

$$\frac{dC(t)}{dt} = -\sum_i k_i C(v_i,t) - \gamma_t (C(t))^2 \tag{4}$$

Parameters $C(t)$ and γ_t are the total particle number concentration (particles cm^{-3}) and the coagulation coefficient ($cm^3\,s^{-1}$), respectively at time t. The first item on the right-hand-side of Eq. (4) describes the particle number concentration decay due to surface deposition while the second one represents the particle loss due to coagulation. The contribution of each process to the total concentration loss changing with time is calculated using Eq. (4).

The size-dependent coagulation rate changes with time and its temporal coagulation rate is difficult to obtain for an aerosol system with varying size and concentration. Therefore, the time-averaged deposition and coagulation rate is calculated using Eq. (5) assuming that γ is a positive constant for the decay of a polydisperse aerosol (Schnell et al., 2006).

$$\frac{C(t)}{C_0} = \frac{k}{(C_0\gamma + k)\ \exp(k\,t) - C_0\gamma} \tag{5}$$

where C_0, k and γ are the initial particle number concentration (particles cm^{-3}), time-averaged overall deposition rate (s^{-1}) and coagulation coefficient ($cm^3\,s^{-1}$), respectively. The values of k and γ are obtained by the least-error-square algorithm and the fitted results almost totally cover the experimental data with a regression coefficient $R^2 > 96\%$ as shown in Table 1. Thus, the parameter k and γ obtained here can describe all the effects on the particle deposition and coagulation, including that of the possible electrostatic charge on the particles.

3.2. Size-resolved deposition rate

The size-resolved deposition rate for 5 target RHs is obtained according to Eq. (1), assuming that the loss of the particles by the sampling process is neglectable compared to those deposited on the wall surfaces of the chamber. The averaged size-resolved deposition rate, k_i, and its standard deviation from the repeated experiments are estimated and listed in Table S3 (see Supporting information). The average deposition rate for each discrete size category at various RHs is shown in Fig. 3. The results confirm a strong size-dependent deposition rate for submicron aerosol particles, in accordance with previous experimental and numerical modeling works (Lee et al., 2014; Zhao et al., 2015; Liu, 2009). Generally, the deposition rate decreases with the size increases for ultrafine particles (< 100 nm) due to Brownian diffusion, and remains low and steady for the particles between 100 and 400 nm, where neither Brownian diffusion nor gravitational settling is dominant. A partially V-shaped curve of deposition rate vs size is observed. The deposition rate for the particles < 30 nm at RH = 27 ± 5%, 39 ± 1%, and 54 ± 3% slightly falls off from the highest point according to the estimated deposition rate of the size-dependent particles (Nazaroff, 2004). This might be attributed to the lower initial concentration of the particles in this size, which causes a seemingly random influence and increases the standard deviation of the analytical method. The highest deposition rate is estimated as 0.403 ± 0.025, 0.322 ± 0.027, 0.295 ± 0.021, 0.292 ± 0.059, and 0.325 ± 0.047 h^{-1} for the RH of 10 ± 5%, 27 ± 5%, 39 ± 1%, 54 ± 3%, and 64 ± 2%, respectively.

In general, the steepness of the size-dependent deposition rate in the decline stage shows a negative relationship with the RH increase. Specifically, for the particles diameter (Dp) < 70 nm, their deposition rate reduces as the RH rises; while for Dp > 70 nm, the deposition rate grows as the RH rises. To the best of our knowledge, no similar investigations have been systemically addressed on the effect of air humidity upon size-resolved particle deposition. A few studies have focused on the micron particle deposition onto ventilation ducts and found that the aerosol deposition is enhanced with the increase of the air humidity (Han et al., 2011; Miguel et al., 2004). However, it has also been suggested that low RH appears to enhance particle deposition of fine particles (Wolkoff and Kjærgaard, 2007). The results in Fig. 3 indicate that RH impacts differently on the particles with different size. This may be attributed to the increase of the viscosity for the moistened air as the air humidity rises, which thickens the viscosity boundary layer near the wall surfaces. Since Brownian diffusion is an important factor to transport ultrafine particles from a homogeneous air in the center to the boundary layer, where the boundary layer thickness controls the nanoparticle deposition onto surfaces directly. Thus, an increasing RH may lead to a slight decrease in the deposition rate by inhibiting the particles transporting to the boundary layer and thicken-

Table 1
Initial conditions, the time-averaged coagulation coefficient and deposition rate for D/C experiments by least-error-square algorithm.

Chamber RH (%)	GMD_0 (nm)	GSD	Coagulation coefficient ($cm^3\,s^{-1}$)	Deposition rate (s^{-1})	R^2
8 ± 2	68.0	1.76	7.98×10^{-11}	1.03×10^{-4}	0.99265
9 ± 3	67.8	1.73	2.69×10^{-10}	9.41×10^{-5}	0.97129
8 ± 3	65.9	1.77	9.61×10^{-12}	1.09×10^{-4}	0.96718
28 ± 2	71.3	1.76	1.88×10^{-9}	2.53×10^{-5}	0.99580
27 ± 2	69.2	1.77	6.82×10^{-10}	8.05×10^{-5}	0.99101
27 ± 1	68.3	1.79	2.10×10^{-9}	1.81×10^{-5}	0.9856
41 ± 1	69.6	1.75	8.93×10^{-10}	7.56×10^{-5}	0.99658
40 ± 1	72.3	1.73	1.95×10^{-9}	2.89×10^{-5}	0.99514
41 ± 1	70.1	1.77	1.45×10^{-9}	6.05×10^{-5}	0.99573
54 ± 1	70.8	1.74	2.49×10^{-9}	3.03×10^{-6}	0.99319
54 ± 1	72.0	1.76	2.78×10^{-9}	3.25×10^{-6}	0.98164
54 ± 1	68.1	1.70	2.62×10^{-9}	1.69×10^{-6}	0.99093
63 ± 1	71.7	1.81	8.91×10^{-10}	8.66×10^{-5}	0.99575
62 ± 2	66.8	1.76	1.20×10^{-9}	6.99×10^{-5}	0.99431
64 ± 1	67.8	1.72	1.69×10^{-9}	2.78×10^{-5}	0.98905

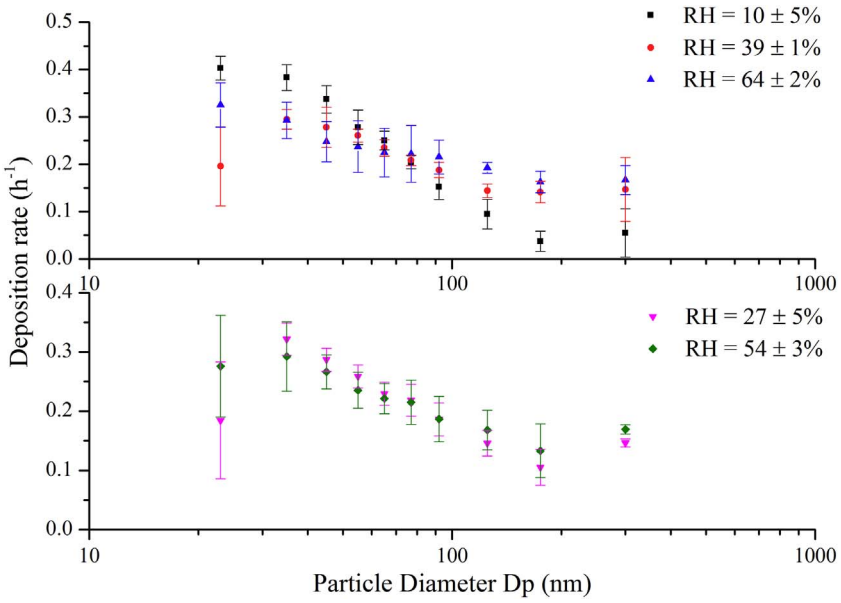

Fig. 3. Estimated deposition rate at different chamber relative humidity (%).

ing the boundary layer. The thickness of the particle concentration boundary layer diminishes significantly with increasing particle diameter (Lai and Nazaroff, 2000). As for the particles (Dp) > 70 nm, an increase of the fluid viscosity with the RH increase and the decrease of the thickness of the particle concentration boundary layer would make the friction velocity larger, and cause the increase of the diffusion and deposition rate (Zhao and Wu, 2007).An increase in the viscosity of the moistened air as well as the rising surface roughness resulted from the water molecules adhere on the wall surfaces may also enhance particle deposition onto the wall (Han et al., 2011).

The comparison of the size-resolved particle deposition rates under still conditions for the particles of 10–1000 nm is depicted in Fig. 4. The experimental parameters such as chamber and particle type, surface-to-volume ratio, chamber RH and the numeric value of k can be found in Table 2. The significant variance of the estimated deposition rate could be attributed to the difference in the chamber shape, surface roughness, surface-to-volume ratio, chemical and physical properties of the particles, and the analytical method used in the model. The chamber RH in previous studies have not been provided, except that the one performed by Zhao et al. (2015) has clearly described the chamber temperature and RH for the gasoline vehicle particle decay tests.

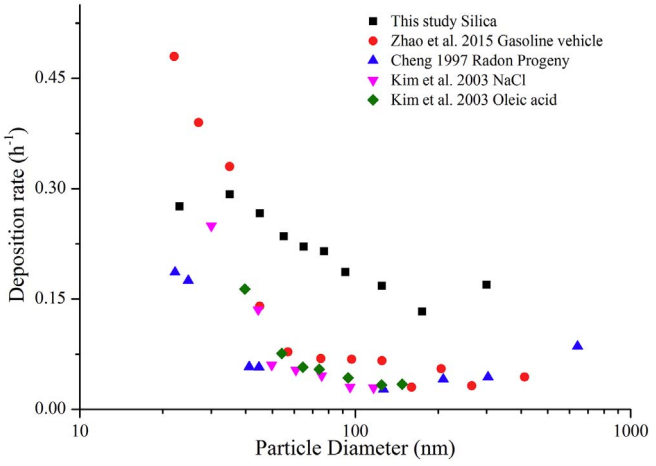

Fig. 4. Comparison of the size-resolved particle deposition rate for various types of nanoparticles under still conditions in the test chamber among this study (RH = 54 ± 3% and T = 25 ± 2 °C) with previous works.

Therefore, the estimated size-resolved deposition rates at RH = 54 ± 3% and T = 25 ± 2 °C from this study and those at T = 25.22 ± 0.15 °C and RH = 54.14 ± 2.25% from Zhao et al.'s (2015) results are used to compare with those reported by others (Schnell et al., 2006; Hussein et al., 2009a; Jamriska and Morawska, 2003; Kim et al., 2003; Cheng, 1997). It is obviously seen that the deposition rate of this study is higher than that of other works for the particles larger than 40 nm. This might owe to a higher surface-to-volume ratio and larger inner surface roughness of our chamber, since the factors is considered to enhance the deposition rate as illustrated by previous researchers (Hussein et al., 2009b). Additionally, the particle deposition is a complicated process involved various behaviors (such as Brownian/turbulent diffusion, gravitational sedimentation, thermophoresis, inertial drift and electrostatic attraction) and can be influenced by a variety of factors (such as the initial particle concentration, the size characteristics, the age and reactivity of the aerosols, temperature, humidity, pressure, and the presence of other volatile gases). These could be the reason for the different results between this study and Zhao et al.'s (2015) one, though the temperature and RH for both researches are quite close. Nevertheless, a general partial V-shaped curve is observed for the submicron particles from the above-mentioned studies, which would benefit to reduce the indoor airborne particle concentration, and thereby the exposure by lowering the percentage of the accumulation mode particles.

3.3. Contribution of the coagulation to total concentration loss

The contribution of the coagulation to the total particle decay is obtained by Eq. (4), based on the size-resolved deposition rate. The exponential regression without boundary conditions is applied to fit the total particle decay over one hour period in high concentration (R^2 > 98%). The geometric mean diameter (GMD) of the particle size distributions increases by 1.16, 1.16, 1.12, 1.14, and 1.14 times during 1 h of the particle decay at RH = 9 ± 4%, 27 ± 3%, 40 ± 1%, 54 ± 1%, and 62 ± 2%, respectively. No significant difference is observed for the particle decay and the size increase under different RH due to close initial concentration that is elaborately controlled by our experiments. Both deposition and coagulation processes are equally important under such circumstances. The calculated average ratio of the coagulation to the total particle loss (CtTPL) at various RHs for the above experiments is exhibited in Fig. 5.

It can be seen that the initial ratio of CtTPL does not exceed 60% at

Table 2
Experimental characteristics and deposition rate for the nanoparticles under still conditions in environmental chambers with the comparable results.

Study	Chamber type	Particle type	S/V[a] (m^{-1})	Chamber RH (%)	Deposition rate (h^{-1})
This study	Polyhedron, stainless steel and PMMA	Spherical SiO_2	8	5–66	0.01–0.40
Zhao et al. (2015)	Cubic, PMMA	Gasoline vehicle exhaust	6	10–54	0.01–0.50
Schnell et al. (2006)	Rectangle, acrylic	Diesel and paper ash	5.25	70	0.01–1.8
Hussein et al. (2009a)	Cubic, aluminum	NaCl salt	6	–	0.03–0.15
Jamriska and Morawska (2003)	Cubic, the inner walls covered with latex paint	Environmental tobacco smoke and petrol	4.5	Under-saturated conditions	0.05–0.10
Cheng (1997)	Spherical, aluminum	Silver and polystyrene latex	8.9	–	0.029–0.17
Kim et al. (2003)	Cylindrical, acrylic box	NaCl and oleic acid	10	–	0.03–0.25

RH 5%–64% and an initial concentration of ~6.0×10^4 particles cm^{-3}. Under the circumstances, the contribution of CtTPL at RH = 27 ± 3%, 40 ± 1%, 54 ± 1%, and 62 ± 2% decreases with its concentration decay with time due to fewer collisions and fewer particle coagulation. Especially for that at a RH of ~54%, a faster decrease of the ratio of CtTPL could be attributed to a higher coagulation rate resulting from the greatly enhanced viscosities of the nanometer-thick water films at the interface (Matthew et al., 2007). Since higher coagulation rate can result in higher particle concentration loss, the CtTPL may vary significantly with time. These trendlines indicating the ratio of CtTPL decreases with time are in agreement with the previous researches (Zhao et al., 2015; Schnell et al., 2006). On the contrary, the ratio of CtTPL at RH = 9 ± 4% slightly increases versus time in the range of 40%–52% assuming the deposition rate does not change with time. The discordance may be attributed to the relatively significant increase in RH (see Fig. S3) from the evaporation of the water molecules adsorbed on the chamber and the possible leakage of the water molecules from the air outside the chamber, which could decrease the surface deposition rate and increase the coagulation coefficient at RH between ~5% and ~30% according to Fig. 6.

In comparison with the previous studies, there are several reasons accounting for the disparities. First, the relative lower initial concentration produces weaker coagulation and is probably the main reason as the initial concentration in this study is about 6.0×10^4 particles cm^{-3} compared with those of 10^5–10^6 particles cm^{-3} in Zhao et al.'s (2015) and Schnell et al.'s (2006) studies, therefore, the contribution of the initial CtTPL is of 40%–60% in this work against those of 85%–90% in their studies. Secondly, different analytical and computational methods may be another reason. Schnell et al. (2006) have determined the ratio of CtTPL by the derived time-averaged coagulation coefficient and deposition rate according to the least-error-square regression method. There must be some deviations between the calculated results and the real values since the transient coagulation rate varies over time. Zhao et al. (2015) have used the best fitting Hamaker constant and the fractal dimension in the coagulation model and the derived friction velocity from Lai and Nazaroff deposition model (2000) to calculate the contribution of CtTPL. The calculation for the transient coagulation rate and the ratio of CtTPL may be more accurate by this method, but is not suitable for this study since it does not fit well with the case at lower initial concentration of ~10^5 particles cm^{-3} at 12.24 °C. Jamriska and Morawska (2003) have reported that the loss rate due to coagulation and surface deposition decreases with time by estimating the deposition rate and the total loss rate via the interpolation method. In this study, we assume that the deposition rate in high-concentration experiments is the same to that in low-concentration ones at similar RHs in order to calculate the ratios of coagulation. Since our experiments are carried out across different seasons, the fluctuating ambient temperature and varying charge status for the aerosols (the aerosols might contact with ambient ions) may also cause the deviations of the deposition rate between differently batched experiments. Nevertheless, the experimental results reveal that the ratio of CtTPL depends on both the initial particle concentration and air humidity. A higher RH incurs a higher initial ratio of CtTPL.

3.4. Time-averaged deposition rate and coagulation coefficient

Fig. 6 shows the time-averaged deposition rate and coagulation coefficient calculated by the least-error-square algorithm at the high-

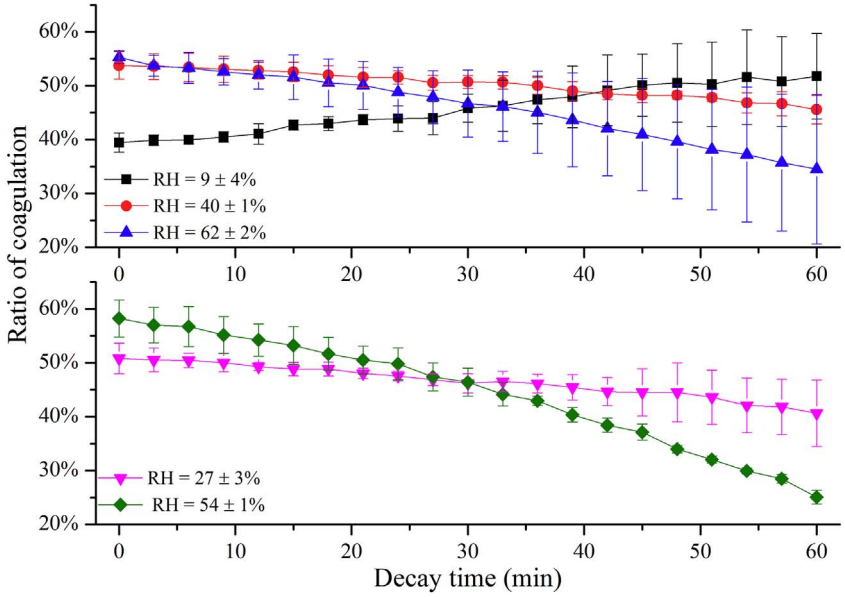

Fig. 5. Contribution of CtTPL during the first 1 h after initial particle decay at diffident relative humidity (%) for D/C experiments.

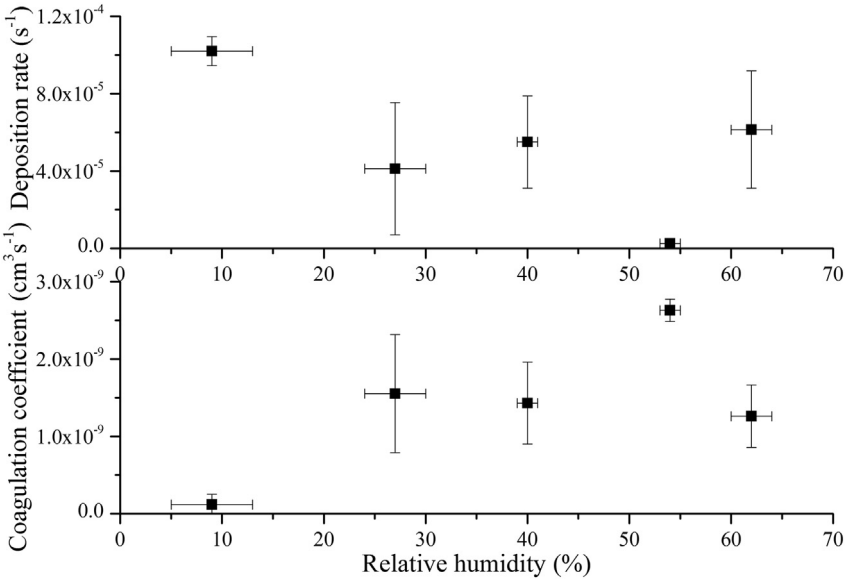

Fig. 6. Time-averaged deposition rate and coagulation coefficient for the D/C experiments calculated by least-error-square algorithm.

Table 3
Experimental characteristics and the coagulation rate for the particles under still conditions with comparable results.

Study	Particle type	Initial GMD_0 (nm)	Investigated time period (s)	Chamber RH (%)	Coagulation rate ($cm^3\ s^{-1}$)
This study	Spherical SiO_2	66–72	3600	5–66	9.61×10^{-12}–2.78×10^{-9}
Schnell et al. (2006)	Diesel and paper ash	52–227	> 6000	70	4.02×10^{-10}–1.01×10^{-8}
Kim et al. (2003)	NaCl	24–115	178–193	–	$(1.01–2.29) \times 10^{-9}$
Chen et al. (1990)	Cigarette smoke	220	2.5	60–95	1.33×10^{-9}
Robinson and Yu (1999)	Cigarette smoke	230	1.4	–	$(1.34–1.70) \times 10^{-9}$

concentration. The experimental conditions for each kind of tests are given in Table 1. It can be seen that the time-averaged deposition rate spans over two orders of magnitude from 10^{-6}–$10^{-4}\ s^{-1}$ and the time-averaged coagulation coefficient spans over three orders of magnitude from 10^{-12}–$10^{-9}\ cm^3\ s^{-1}$. Comparisons of the deposition rate and coagulation coefficient among this study and those found in the literature (Schnell et al., 2006; Hussein et al., 2009a; Jamriska and Morawska, 2003; Kim et al., 2003; Cheng, 1997; Chen et al., 1990; Robinson and Yu, 1999) are illustrated in Tables 2 and 3, respectively. The results show that the deposition rate is slightly higher and the coagulation one is slightly lower than those by other researches. It suggests that, due to the larger ratio of surface area-to-volume for the chamber, electrostatic losses to the chamber wall, if any, might account for a significant amount of the deposition loss at RH = 9 ± 4%. The derived coagulation coefficient in this study is slightly lower than those reported by other investigators and probably caused by the different initial particle concentration, size distribution, residence time and chamber RH, etc.

We compare the derived time-averaged deposition rate and coagulation coefficient at different RHs as shown in Fig. 6. The horizontal error bars represent the standard deviations for the actual RHs recorded by the instrument and the vertical error bars implicate the spread width of the coagulation coefficients calculated at each RH. It could roughly concludes that the RH has an effect on the particle D/C, where the highest deposition rate and the lowest coagulation coefficient occur at RH = 9 ± 4%, while the lowest deposition rate and the highest coagulation coefficient emerge at RH = 54 ± 1%. This is consistent with the fact that the particles adhere to other particles more strongly as the humidity increases (Miguel, 2003). Surface tension due to water molecular adsorption on the –OH groups of SiO_2 NPs is a potential cause for the increasing coagulation coefficient at high RH, which results in the formation of nanometer-thick water films and the great increase of the viscosity (Matthew et al., 2007), like that of the interaction of the H_2O molecules with the salt surface (Wise et al., 2008; Darr et al., 2014; Bruzewicz et al., 2011). The slightly higher initial concentration at RH = 27 ± 3% and 54 ± 1% probably lead to the coagulation rate higher than those at RH = 40 ± 1% and 62 ± 2%, respectively. Though the effect of the RH on the particle deposition and coagulation is relatively weak when compared with that of the particle size and the second order relationship between the coagulation and the transient concentration, it cannot be ignored when considering the environmental safety of the nanoparticles and the potential risks for human exposure.

Electrostatic charge on the particles and walls may significantly influence their deposition rate. In this study, a soft X-ray neutralizer is used to balance the charges on the particles in each experiment. However, considerable standard deviations of the deposition rate and coagulation coefficient still exist despite of the use of the well-defined nanoparticles. Another effect such as the acquired electrostatic charges due to the contacts between the nanoparticles and the ambient ions may cause a random influence. Especially at RH = 9 ± 4%, the aerosolized nanoparticles might be charged to a great extent under such a dry condition than those under humid condition such as RH = 27 ± 3%, 40 ± 1%, 54 ± 1%, and 62 ± 2%. The highest deposition rate occurred at RH = 9 ± 4% may owe to the mutual repulsion among particles and attraction between the particles and the metal wall due to the induced opposite charges by the approaching particles (Foster, 1959). With no doubt, other factors, such as the variation of temperature may also be a reason for the variation of deposition rate and coagulation coefficient, but the effect of temperature needs to be considered separately and is beyond the scope of this paper.

4. Conclusion

The main focus of this paper is on the assessment of the effect of the RH on the surface deposition and coagulation with reducing number concentration of the aerosolized nanoparticles under still conditions without considering other interactions. Experiments are conducted in an enclosed chamber to measure the size distributions and particle concentration decay for the ultrafine particles with time. Initial number concentrations below 2.0×10^4 particles cm^{-3} are used to evaluate the deposition-only process, and $\sim 6.0 \times 10^4$ particles cm^{-3} are used to study that with simultaneous coagulation and deposition in the chamber, respectively. Three evaluation methods are applied to obtain the size-resolved deposition rate, the contribution of CtTPL, and the time-averaged deposition rate and coagulation coefficient.

The experimental results reveal that the RH has an obvious effect on the size-resolved deposition rate and coagulation coefficient for the airborne nanoparticles, which cannot be neglected. First, the impact of the RH on the size-resolved deposition rate depends on particle size; for $Dp < 70$ nm, the deposition rate decreases as the RH rises; while for $Dp > 70$ nm, the deposition rate grows as the RH rises. Secondly, the change of the ratio of CtTPL varies with the initial particle concentration and air humidity; for the initial particle concentration of $\sim 6.0 \times 10^4$ particles cm^{-3}, the ratio of CtTPL does not exceed 60%; and the high initial ratio of CtTPL tends to be associated with the high RH conditions, which may lead to the formation of nanometer-thick water films at the interface and enhance the viscosities greatly. Thirdly, the minimum time-averaged deposition rate and the maximum coagulation coefficient appear at RH ~54%; both the lower and higher RH conditions tend to enhance the deposition rate of the nanoparticles; the coagulation coefficient of the nanoparticles increases with the increased humidity due to strong inter-particle adherence.

Due to the variation in each experiment, such as the temperature, the charge state on the particles and walls of the chamber, the deposition rate and coagulation coefficient obtained in this study may not be directly applicable to real-world simulations. Except for the experimental errors, systematic errors would also be caused by the modeling. However, the statistic results from this article provides an estimation for the RH influence on the surface deposition and coagulation, which can be used to assess the indoors ENP behavior and their potential risks to human exposure.

Acknowledgements

The authors gratefully acknowledge funding of the project “Industrial Nano-manufacturing Focus” by Chinese Academy of Sciences (XDA09040400) and the funding by Ministry of Science and Technology of the People's Republic of China (2016YFA0200900).

Appendix A. Supplementary data

Supplementary data to this article can be found online at http://dx.doi.org/10.1016/j.atmosres.2017.04.030.

References

Allard, F., Dorer, V., Feustel, H.E., Garcia, E., Grosso, M., Herrlin, M., Mingsheng, L., Phaff, J., Utsumi, Y., Yoshino, H., 1990. Fundamentals of the Multizone Air Flow Model-COMIS. Air Infiltration and Ventilation Centre, Coventry, UK.

Bräuner, E.V., Forchhammer, L., Møller, P., Simonsen, J., Glasius, M., Wåhlin, P., Raaschou-Nielsen, O., Loft, S., 2007. Exposure to ultrafine particles from ambient air and oxidative stress-induced DNA damage. Environ. Health Perspect. 115, 1177–1182.

Bruzewicz, D.A., Checco, A., Ocko, B.M., Lewis, E.R., Mcgraw, R.L., Schwartz, S.E., 2011. Reversible uptake of water on NaCl nanoparticles at relative humidity below deliquescence point observed by noncontact environmental atomic force microscopy. J. Chem. Phys. 134, 044702.

Buesser, B., Heine, M., Pratsinis, S., 2009. Coagulation of highly concentrated aerosols. J. Aerosol Sci. 40, 89–100.

Chen, B.T., Namenyi, J., Yeh, H.C., Mauderly, J.L., Cuddihy, R.G., 1990. Physical characterization of cigarette smoke aerosol generated from a Walton smoke machine. Aerosol Sci. Technol. 12, 364–375.

Chen, L., Tian, G.L., Wang, Y.F., Ge, G.L., 2016. “A one-step controlled synthesis of mono-, bi-, tri- and poly-disperse SiO_2 aerosol nano- and micro-spheres”, Patent, Application No. 201610807762.1.

Cheng, Y.S., 1997. Wall deposition of radon progeny and particles in a spherical chamber. Aerosol Sci. Technol. 27, 131–146.

Darr, J.P., Davis, S.Q., Kohno, Y., Mckenna, K., Morales, P., 2014. Morphological effects on the hygroscopic properties of sodium chloride-sodium sulfate aerosols. J. Aerosol Sci. 77, 158–167.

Foster, W.W., 1959. Deposition of unipolar charged aerosol particles by mutual repulsion. Br. J. Appl. Phys. 10, 206–213.

Friedlander, S.K., Pui, D.Y., 2004. Emerging issues in nanoparticle aerosol science and technology. J. Nanopart. Res. 6, 313–320.

Guo, Z., 2000. Simulation Tool Kit for Indoor Air Quality and Inhalation Exposure (IAQX) User's Guide, Version 1.0, EPA-600/R-00-094. National Risk Management Research Laboratory, United States Envrionmental Protection Agency, Research Triangle Park, NC, USA.

Han, Y., Hu, Y., Qian, F., 2011. Effects of air temperature and humidity on particle deposition. Chem. Eng. Res. Des. 89, 2063–2069.

Hinds, W.C., 1999. Aerosol Technology: Properties, Behavior, and Measurement of Airborne Particles, second ed. John Wiley & Sons, New York.

Hussein, T., Hruška, A., Dohányosová, P., Džumbová, L., Hemerka, J., Kulmala, M., Smolík, J., 2009a. Deposition rates on smooth surfaces and coagulation of aerosol particles inside a test chamber. Atmos. Environ. 43, 905–914.

Hussein, T., Kubincová, L., Džumbová, L., Hruška, A., Dohányosová, P., Hemerka, J., Smolik, J., 2009b. Deposition of aerosol particles on rough surfaces inside a test chamber. Build. Environ. 44, 2056–2063.

Jamriska, M., Morawska, L., 2003. Quantitative assessment of the effect of surface deposition and coagulation on the dynamics of submicrometer particles indoors. Aerosol Sci. Technol. 37, 425–436.

Jamriska, M., Morawska, L., Mergersen, K., 2008. The effect of temperature and humidity on size segregated traffic exhaust particle emissions. Atmos. Environ. 42, 2369–2382.

Jiang, R.X., Tan, H.B., Tang, L.L., Cai, M.F., Yin, Y., Li, F., Liu, L., Xu, H.B., Chan, P.W., Deng, X.J., Wu, D., 2016. Comparison of aerosol hygroscopicity and mixing state between winter and summer seasons in Pearl River Delta region, China. Atmos. Res. 169, 160–170.

Kim, D., Park, S., Song, Y., Kim, D., Lee, K., 2003. Brownian coagulation of polydisperse aerosols in the transition regime. J. Aerosol Sci. 34, 859–868.

Lai, A.C., 2002. Particle deposition indoors: a review. Indoor Air 12, 211–214.

Lai, A.C., Nazaroff, W.W., 2000. Modeling indoor particle deposition from turbulent flow onto smooth surfaces. J. Aerosol Sci. 31, 463–476.

Lee, K., Chen, H., 1984. Coagulation rate of polydisperse particles. Aerosol Sci. Technol. 3, 327–334.

Lee, W.C., Wolfson, J.M., Catalano, P.J., Rudnick, S.N., Koutrakis, P., 2014. Size-resolved deposition rates for ultrafine and submicrometer particles in a residential housing unit. Environ. Sci. Technol. 48, 10282–10290.

Liu, D.-L., 2009. Particle deposition onto enclosure surfaces. In: Kohli, R., Mittal, K.L. (Eds.), Developments in Surface Contamination and Cleaning: Particle Deposition, Control and Removal. Elsevier, Amsterdam (2010).

Liu, P.F., Zhao, C.S., Gobel, T., Hallbauer, E., Nowak, A., Ran, L., Xu, W.Y., Deng, Z.Z., Ma, N., Mildenberger, K., Henning, S., Stratmann, F., Wiedensohler, A., 2011. Hygroscopic properties of aerosol particles at high relative humidity and their diurnal variations in the North China Plain. Atmos. Chem. Phys. 11, 3479–3494.

Martin, J., Bello, D., Bunker, K., Shafer, M., Christiani, D., Woskie, S., Demokritou, P., 2015. Occupational exposure to nanoparticles at commercial photocopy centers. J. Hazard. Mater. 298, 351–360.

Matthew, P.G., Houston, J.E., Zhu, X.Y., 2007. Hydrophilicity and the viscosity of interfacial water. Langmuir 23, 5491–5497.

Maynard, A.D., Zimmer, A.T., 2003. Development and validation of a simple numerical model for estimating workplace aerosol size distribution evolution through coagulation, settling, and diffusion. Aerosol Sci. Technol. 37, 804–817.

Miguel, A.F., 2003. Effect of air humidity on the evolution of permeability and performance of a fibrous filter during loading with hygroscopic and non-hygroscopic particles. J. Aerosol Sci. 34, 783–799.

Miguel, A.F., Reis, A.H., Aydin, M., 2004. Aerosol particle deposition and distribution in bifurcating ventilation ducts. J. Hazard. Mater. 116, 249–255.

Montgomery, J.F., Green, S.I., Rogak, S.N., 2015a. Impact of relative humidity on HVAC filters loaded with hygroscopic and non-hygroscopic particles. Aerosol Sci. Technol. 49, 322–331.

Montgomery, J.F., Rogak, S.N., Green, S.I., You, Y., Bertram, A.K., 2015b. Structural change of aerosol particle aggregates with exposure to elevated relative humidity. Environ. Sci. Technol. 49, 12054–12061.

Morawska, L., Jamriska, M., Bofinger, N.D., 1997. Size characteristics and ageing of the environmental tobacco smoke. Sci. Total Environ. 196, 43–55.

Nazaroff, W.W., 2004. Indoor particle dynamics. Indoor Air 14, 175–183.

Ostraat, M.L., Swain, K.A., Small, R.J., 2010. Insight into the behavior of engineered aerosolized nanoparticles. Int. J. Occup. Environ. Health 16, 458–466.

Otto, E., Fissan, H., Park, S., Lee, K., 1999. The log-normal size distribution theory of Brownian aerosol coagulation for the entire particle size range: part II—analytical solution using Dahneke's coagulation kernel. J. Aerosol Sci. 30, 17–34.

Rim, D., Green, M., Wallace, L., Persily, A., Choi, J.-I., 2012. Evolution of ultrafine particle size distributions following indoor episodic releases: relative importance of coagulation, deposition and ventilation. Aerosol Sci. Technol. 46, 494–503.

Robinson, R.J., Yu, C.P., 1999. Coagulation of cigarette smoke particles. J. Aerosol Sci. 30, 533–548.

Schnell, M., Cheung, C., Leung, C., 2006. Investigation on the coagulation and deposition of combustion particles in an enclosed chamber with and without stirring. J. Aerosol Sci. 37, 1581–1595.
Sotiriou, G.A., Singh, D., Zhang, F., Wohlleben, W., Chalbot, M.-C.G., Kavouras, I.G., Demokritou, P., 2015. An integrated methodology for the assessment of environmental health implications during thermal decomposition of nano-enabled products. Environ. Sci.: Nano 2, 262–272.
Stölzel, M., Breitner, S., Cyrys, J., Pitz, M., Wölke, G., Kreyling, W., Heinrich, J., Wichmann, H.-E., Peters, A., 2007. Daily mortality and particulate matter in different size classes in Erfurt, Germany. J. Expo. Sci. Environ. Epidemiol. 17, 458–467.
Wehner, B., Birmili, W., Gnauk, T., Wiedensohler, A., 2002. Particle number size distributions in a street canyon and their transformation into the urban-air background: measurements and a simple model study. Atmos. Environ. 36, 2215–2223.
Wise, M.E., Martin, S.T., Russell, L.M., Buseck, P.R., 2008. Water uptake by NaCl particles prior to deliquescence and the phase rule. Aerosol Sci. Technol. 42, 281–294.
Wolkoff, P., Kjærgaard, S.K., 2007. The dichotomy of relative humidity on indoor air quality. Environ. Int. 33, 850–857.
Yu, M., Koivisto, A.J., Hämeri, K., Seipenbusch, M., 2013. Size dependence of the ratio of aerosol coagulation to deposition rates for indoor aerosols. Aerosol Sci. Technol. 47, 427–434.
Zhao, B., Wu, J., 2007. Particle deposition in indoor environments: analysis of influencing factors. J. Hazard. Mater. 147, 439–448.
Zhao, Y., Wang, F., Zhao, J., 2015. Size-resolved ultrafine particle deposition and Brownian coagulation from gasoline vehicle exhaust in an environmental test chamber. Environ. Sci. Technol. 49, 12153–12160.